In Vivo Tumor Grading of Prostate Cancer Using ^{111}In-Capromab Pendetide SPECT/CT

Youngho Seo[1–3], Carina Mari Aparici[1,4], Matthew R. Cooperberg[4,5], Badrinath R. Konety[4,5], and Randall A. Hawkins[1,2]

[1]Department of Radiology and Biomedical Imaging, University of California, San Francisco, California; [2]Joint Graduate Group in Bioengineering, University of California, San Francisco and Berkeley, California; [3]Department of Radiation Oncology, Helen Diller Family Comprehensive Cancer Center, University of California, San Francisco, California; [4]San Francisco Veterans Affairs Medical Center, San Francisco, California; and [5]Department of Urology, University of California, San Francisco, California

We have developed an in vivo method to quantify antibody uptake using ^{111}In-capromab pendetide SPECT combined with CT (SPECT/CT). Our goal was to evaluate this method for potential grading of prostate tumors. **Methods:** Our phantom experiments focused on the robustness of an advanced iterative reconstruction algorithm that involves corrections for photon attenuation, scatter, and geometric blurring caused by radionuclide collimators. The conversion factors between image values and tracer concentrations (in Bq/mL) were calculated from a uniform phantom filled with an aqueous solution of $^{111}InCl_3$ using the same acquisition protocol and reconstruction parameters as for patient studies. In addition, the spatial resolution of the reconstructed images was measured from a point source phantom. The measured spatial resolution was modeled into a point-spread function, and the point-spread function was implemented in a deconvolution-based partial-volume-error correction algorithm. The recovery capability to correctly estimate true tracer concentrations was tested using prostatelike and bladderlike lesion phantoms fitted in the modified National Electrical Manufacturers Association/International Electrotechnical Commission body phantom. Patients with biopsy-proven prostate cancer (n = 10) who underwent prostatectomy were prospectively enrolled in the preoperative SPECT/CT studies at the San Francisco Veterans Affairs Medical Center. The CT portion of SPECT/CT was used to generate CT-based attenuation maps and as an anatomic localization tool for clinical interpretation. Pathologic Gleason grades were compared with in vivo antibody uptake value (AUV) normalized by injected dose, effective half-life, and injection-scan time difference. AUVs were calculated in each lobe of the prostate gland with cylindric volumes of interest having dimensions of 1.5 cm in both diameter and height. **Results:** Reconstructed SPECT images further corrected by the deconvolution-based partial-volume-error correction could recover tracer concentrations up to 90% of true values in measurements of phantom volumes as small as 7.77 mL. From patient studies, there was a statistically significant correlation (ρ = 0.71, P = 0.033) between higher AUVs (from either left or right lobe) and higher components of pathologic Gleason scores. **Conclusion:** Our results strongly indicate potential for noninvasive prostate tumor grading using quantitative ^{111}In-capromab pendetide SPECT/CT.

Key Words: prostate cancer; capromab pendetide; SPECT; SPECT/CT; quantification; tracer quantification; quantitative SPECT; prostate-specific membrane antigen (PSMA)

J Nucl Med 2010; 51:31–36
DOI: 10.2967/jnumed.109.067108

SPECT and PET are widely used noninvasive molecular imaging tools (*1*). Although the application of either imaging modality depends on the availability of useful radiotracers, PET always has been preferred when the quantitative accuracy of the result is a particularly important component for a given application (*2*). In most existing applications, SPECT is less precise primarily because of its lower photon statistics, compared with those of PET. In addition, physical correction techniques for photon attenuation, scatter, and geometric blurring caused by radionuclide collimators are not fully implemented or validated in typical SPECT applications (*3*); thus, truly quantitative SPECT for tracer quantification is seldom used.

Of many potential SPECT applications, the SPECT diagnostic evaluation of prostate cancer metastasis can be greatly enhanced with tracer quantification. ^{111}In-capromab pendetide is a monoclonal antibody targeting prostate-specific membrane antigen (PSMA) labeled with ^{111}In that emits high-energy photons suitable for SPECT (*4*). Conventional use of ^{111}In-capromab pendetide SPECT does not require any quantification because the imaging is used mainly to image sites of disease (*5*).

Immunohistochemical staining with the PSMA-targeting 7E11-C5 monoclonal antibody, the antibody for ^{111}In-capromab pendetide, is more intense in malignant prostate tissue than in benign tissue and is positive in lymph node and bony metastases (*6*). In addition, in specimens obtained

Received Jun. 8, 2009; revision accepted Oct. 7, 2009.
For correspondence contact: Youngho Seo, Department of Radiology and Biomedical Imaging, University of California, San Francisco, CA 94143-0946.
E-mail: youngho.seo@radiology.ucsf.edu

from patient studies, PSMA expression using 7E11-C5 immunohistochemical staining has been found to be generally higher in primary cancer and lymph node metastases than in benign epithelium (*7*). However, in vivo PSMA expression using ^{111}In-capromab pendetide SPECT or any other imaging method has never been correlated with tumor aggressiveness. Conventional use of ^{111}In-capromab pendetide SPECT never required any quantification because imaging was mainly used for evaluation of spread of disease (*5*). To date, however, concerns about lack of specificity have limited the widespread clinical applicability of standard ^{111}In-capromab pendetide–based imaging.

We demonstrate how tracer quantification through quantitative SPECT enables correlation between in vivo PSMA expression as determined from imaging and pathologic tumor grade. Our approaches to tracer quantification primarily focus on combined SPECT/CT technology (*8*), which provides practical procedures for photon attenuation correction of ^{111}In data (*9*). We also use corrections for photon scatter and geometric blurring caused by radionuclide collimators for SPECT image reconstruction (*9–11*). Our approach is in line with some previous efforts using CT-based corrections in iterative SPECT reconstruction algorithms to obtain better quantitative accuracies for reconstructed concentrations in comparison to correction methods based on SPECT transmission scans (*12*). Of particular note is that correct implementation of attenuation correction was found to be a significant factor in achieving artifact-free SPECT images (*13*) and in improving quantitative information on radioactivity distribution (*14*). However, with regard to tracer quantification within small volumes of interest (e.g., prostate glands), we further used an additional postreconstruction partial-volume technique we originally developed for PET images to obtain improved quantitative information on tracer concentrations (*15*). As a result, after careful phantom-calibration evaluations, we were able to convert pixel values in SPECT reconstructed volumes into tracer concentrations (Bq/mL). Using the tracer concentrations normalized by appropriate patient-specific imaging variables such as injected dose and interval between injection and scan times, we evaluated the correlation of in vivo PSMA expression with pathologic tumor grade from prospectively enrolled prostate cancer patients who underwent radical prostatectomy after SPECT/CT.

MATERIALS AND METHODS

SPECT/CT Acquisition and Reconstruction Parameters

All our studies used a commercially available SPECT/CT scanner (Precedence, with a 0.9525-cm [3/8-in] NaI(Tl) crystal thickness and a 16-slice multidetector CT component; Philips Healthcare) installed at San Francisco Veterans Affairs Medical Center. All SPECT data in both phantom and patient studies were acquired using a 128 × 128 matrix with a 4.664-mm pixel size using medium-energy general-purpose collimators. The SPECT acquisition was performed with 64 stops (128 angles by 2 camera heads) at 55 s per stop for a 360° rotation. SPECT reconstructions were performed using an algorithm involving CT-based attenuation correction, and scatter and geometric blurring corrections (Astonish; Philips Healthcare) with 12 iterations and 8 subsets of ordered-subsets expectation maximization. The postprocessing filter of reconstructed images was Hanning with a 1.5 cutoff frequency. In case there was a visual mismatch between the CT attenuation map and the SPECT emission data, the 2 data were manually registered before reconstruction of the final SPECT images. Using the JETStream workstation provided by the scanner manufacturer, each SPECT reconstruction took approximately 30 min each. For patient studies, approximately 185 MBq (5 mCi) of ^{111}In-capromab pendetide were administered intravenously, followed by the SPECT/CT acquisitions at approximately 96 h after injection. The helical CT was performed without iodinated contrast agent using the manufacturer's default CT attenuation correction acquisition parameters. The CT data were reconstructed using a filtered backprojection algorithm provided by the scanner manufacturer.

Phantom Preparation

To calculate radiotracer concentrations (Bq/mL) in each voxel of SPECT reconstructed volumes, we performed a SPECT/CT scan of phantoms that were divided into 3 parts: uniform volume, point source, and small and large volumetric lesions. All 3 parts of the phantoms were fit within 1 SPECT field of view to minimize the number of scans needed. The uniform volume was created by partial filling of an aqueous solution of $^{111}InCl_3$ (53.65 MBq) to test the uniformity of the reconstructed SPECT image and to calculate a conversion factor from voxel values (arbitrary unit) to radiotracer concentrations (Bq/mL). The partial-filling technique was used to ensure complete mixing of the $^{111}InCl_3$ aqueous solution for the uniformity test. The point source was simulated using a drop of $^{111}InCl_3$ solution within a small centrifuge tube. This point source was used to measure the spatial resolution of reconstructed SPECT images. The point-spread function was estimated from the spatial resolution value and was an input parameter to the previously developed postreconstruction partial-volume-error (PVE) correction algorithm (*15,16*). This PVE correction algorithm iteratively compensates PVEs of spill-ins and spill-outs from neighboring pixels by deconvolving the reconstructed volume with the measured point-spread function. The small and large lesions were simulated in phantoms as for prostate gland and bladder and to test our physical correction techniques and PVE correction algorithm to recover known tracer concentrations.

The modified National Electrical Manufacturers Association/International Electrotechnical Commission (NEMA/IEC) body phantom to include bladderlike (146 mL) and prostatelike (7.77 mL) lesions filled with $^{111}InCl_3$ aqueous solution was prepared in the radiopharmacy laboratory at San Francisco Veterans Affairs Medical Center. At scanning time, activity concentrations for the bladderlike and prostatelike lesions were 32.9 kBq/mL and 636.3 kBq/mL, respectively. The rest of the parts in the body phantom—the body and 6 spheres—were filled with nonradioactive water to simulate attenuation medium. Before phantom filling, all doses were measured using a dose calibrator calibrated for ^{111}In. Once the phantom compartments were filled with radioactivity, leak-proof covers and screws were fastened and the phantom was agitated to ensure complete mixing of $^{111}InCl_3$ with water at room temperature. The bladderlike and prostatelike lesions were manufactured in the investigators' own machine shop at the University of California, San Francisco and were fit in the standard NEMA/IEC body phantom (*17*).

Patient Recruitment and Pathologic Analysis

Patients were recruited after an institutional review board approved the protocol for collecting image data and other test results related to the imaging studies, including descriptive pathologic evaluation after prostatectomy. Other than the eligibility of prostatectomy, no other restrictive patient selection criteria were imposed.

Advanced Reconstruction and Deconvolution Techniques on Patient Images

We focused on tracer quantification in small volumes such as the prostate gland. In addition, as far as the spatial resolution of ^{111}In-SPECT/CT allows, our goal is to develop quantitative indices for each lobe of the prostate gland. Given the often-multicentric distribution of prostate cancer in the gland, even left/right quantitative indices should be useful in characterizing disease. Our choice of reconstruction parameters was based on a preliminary study in which an extra correction term such as attenuation correction in an iterative reconstruction algorithm requires typically twice the iterations to maintain the same signal-to-noise ratio before and after inclusion of the extra correction term (*10*). Therefore, including CT-based photon attenuation correction and geometric blurring correction as well as scatter correction, we chose 12 iterations—6 times the manufacturer's default number of 2 iterations—of the ordered-subsets expectation maximization algorithm when these 3 correction terms are not included. This advanced reconstruction algorithm was necessary to present good image quality for interpretation of ^{111}In-capromab pendetide SPECT/CT studies. The measured spatial resolution was an average of 9 mm in full width at half maximum (FWHM).

However, for tracer quantification within the prostate gland, our volumes of interest were 2 identical cylinders having dimensions of 1.5 cm in both diameter and height at each side of the prostate gland. The volume of interest was smaller than twice the FWHM. Our deconvolution-based postreconstruction PVE correction was necessary to further tighten the errors associated with tracer concentration estimates. Figure 1 illustrates this tightening effect. The top images are before the application of the deconvolution-based PVE correction in transaxial and coronal views; the bottom images are after the PVE correction.

Antibody Uptake Value (AUV) Correlation with Tumor Grade

The cylindric volumes of interest were drawn completely within each lobe of the prostate gland to calculate the mean value of tracer concentrations in Bq/mL. The tracer concentrations were converted to AUV, which is similar to the standardized uptake value (*18*) commonly used in PET quantitation. However, AUV is not normalized by individual patient weight because in vivo uptake of antibody such as 7E11-C5 in ^{111}In-capromab pendetide is a biochemical characteristic at the level of tissue, which should not vary significantly with patient weight. AUVs were calculated from preoperative data on the prospectively enrolled 10 patients using the following formula:

$$\text{AUV (Bq/mL/MBq)} = \frac{C'(t_s)\cdot e^{\lambda_{eff}(t_s - t_i)}}{A(t_i)}, \qquad \text{Eq. 1}$$

where $C'(t_s)$ is activity concentration (Bq/mL) estimated using the conversion factor from the uniformity measurement and corrected with the 9 mm FWHM iterative deconvolution algorithm,

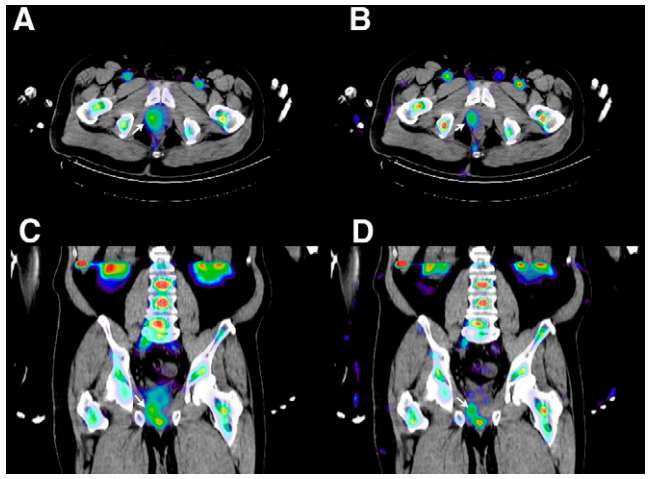

FIGURE 1. Effect of deconvolution-based PVE correction on reconstructed SPECT/CT images. Transaxial (top row) and coronal (bottom row) views before (A) and after (B) PVE correction are shown. Arrows indicate areas of uptake (prostate gland) showing improved spatial resolution after PVE correction.

λ_{eff} is the effective decay constant of ^{111}In-capromab pendetide (0.01034 h^{-1}), t_s is the scan time, t_i is the injection time (in h), and $A(t_i)$ is the total activity injected (in MBq). AUV is given in Bq/mL/MBq because this unit provides a user-friendly range of values typically between 20 and 100.

After these AUVs were calculated from patients who went through radical prostatectomy and anatomic pathologic examination after the surgical procedure, we obtained pathologic tumor grades from all these patients. The pathologic Gleason score is often a valuable prognostic factor in prostate cancer management (*19*). The Gleason grading system assigns a grade from 1 (very well differentiated) to 5 (very poorly differentiated) to the most dominant and second most dominant histologic patterns (*20*). Comparison was made between higher AUVs (either left lobe or right lobe) and higher grade of the Gleason score because given the limitations of the imaging test in terms of not having finer spatial resolution, smaller segmentation of AUV measurements is difficult to justify. The higher grade of the Gleason score was chosen assuming high AUV can be closely related to intensive PSMA overexpression. As shown in Figure 2, the higher Gleason grade from our 10-patient datasets was either 3 (from 3 + 3 Gleason score) or 4 (either from 3 + 4 or from 4 + 3).

RESULTS

^{111}In Concentration Calculation from Small Volumes

The uniform volume after reconstruction using the iterative ordered-subsets expectation maximization algorithm that involved CT-based attenuation correction, scatter correction, and geometric blurring correction resulted in a reconstructed SPECT image with the uniform line profile shown in Figure 3. This line profile was obtained from a transaxial slice stacked over 20 uniform slices. From this measurement, the conversion factors as multiplication factors from the reconstructed image value (arbitrary unit) to the activity concentration (Bq/mL) were estimated as

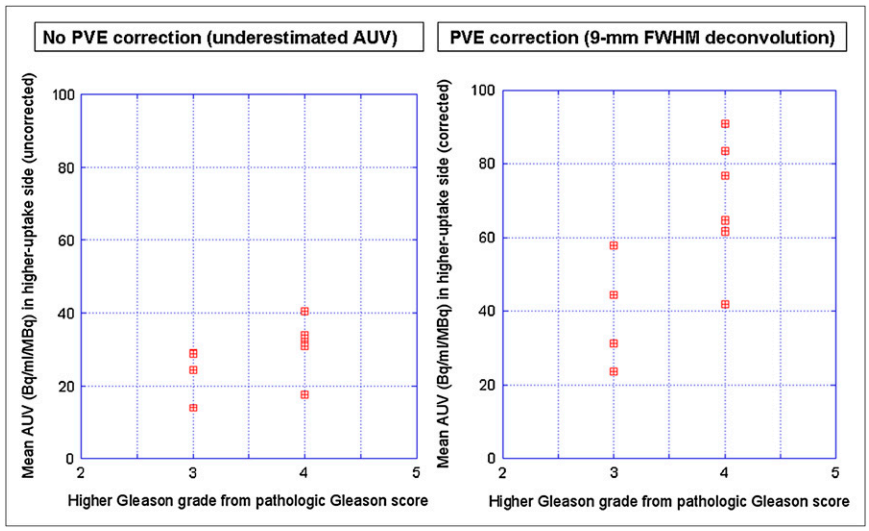

FIGURE 2. Correlation plots of AUVs against Gleason tumor grades from data of 10 patients who underwent preoperative ^{111}In-capromab pendetide SPECT/CT and prostatectomy. Gleason tumor grades were obtained from pathologic examination of prostatectomy samples. AUVs were calculated before and after deconvolution-based PVE correction had been applied.

9.87 and 13.31 for PVE-uncorrected images and PVE-corrected images, respectively. The reconstructed point-source image resulted in an average FWHM of 9 mm using gaussian function fits in all 3 cartesian coordinates. The average FWHM was a mean of 3 values corresponding to 3 cartesian coordinates. Thus, after applying the 9 mm FWHM point-spread function to our iterative deconvolution technique to correct for PVEs as well as the conversion factor from the uniform phantom, we could recover activity concentrations (in Bq/mL) up to approximately 90% of true values in a small prostatelike lesion (7.77 mL) and up to almost 100% of true values in a large bladderlike lesion (146 mL). Figure 4 shows that our PVE correction technique outperforms the non-PVE correction conversion method in the concentration value recovery process.

SPECT/CT Images of Patients After Advanced Corrective Reconstruction

Figure 1 illustrates this tightening effect. This example shows how the deconvolution-based PVE correction algorithm was necessary to quantify a small volume such as the prostate gland because even the reconstruction algorithm that incorporated photon attenuation, scatter, and collimator response corrections could not provide the necessary spatial resolution to draw values in small volumes of interest. Blurring of the tracer distribution in the prostate gland was significantly improved after the PVE correction was applied.

AUV Correlation with Tumor Grade

Figure 2 shows the correlations between AUVs and Gleason grades of tumors. As the figure indicates, the deconvolution-based PVE correction provides a statistically more significant correlation between the 2 values. The potential result is that ^{111}In-capromab pendetide SPECT/CT might be used as an in vivo tumor-grading tool. The Spearman rank correlation test shows that correlation coefficients were $\rho = 0.64$ and 0.71 for Gleason tumor grade correlation with PVE-uncorrected AUVs and with PVE-corrected AUVs, respectively. The 2-sided P values were 0.055 and 0.033, respectively. Hence, if we consider the statistical significance with a P value of less than 0.05, the deconvolution-based PVE correction needs to be applied to make the correlation results statistically significant using our limited sample size ($n = 10$).

DISCUSSION

The use of conversion factors to estimate activity concentrations in Bq/mL is routinely applied in PET but

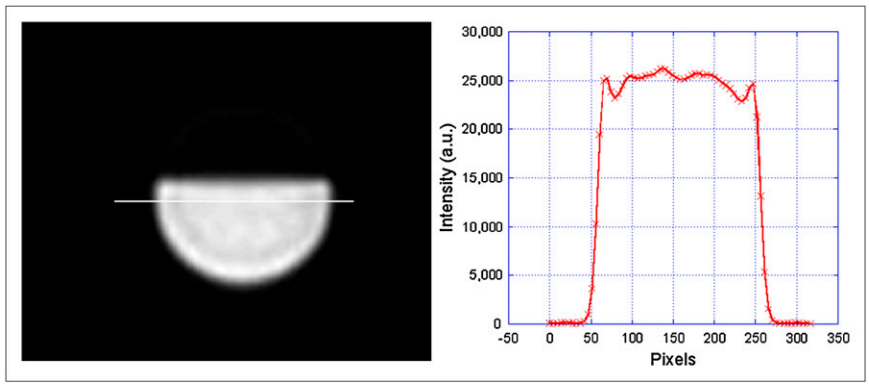

FIGURE 3. Reconstructed uniform phantom image in transaxial view. Phantom was cylindric. Aqueous solution of $^{111}InCl_3$ was mixed with water, and the cylindric volume was partially filled to ensure complete mixing with water. Line profile shows fairly uniform intensity pattern except for small dips near edge close to wall.

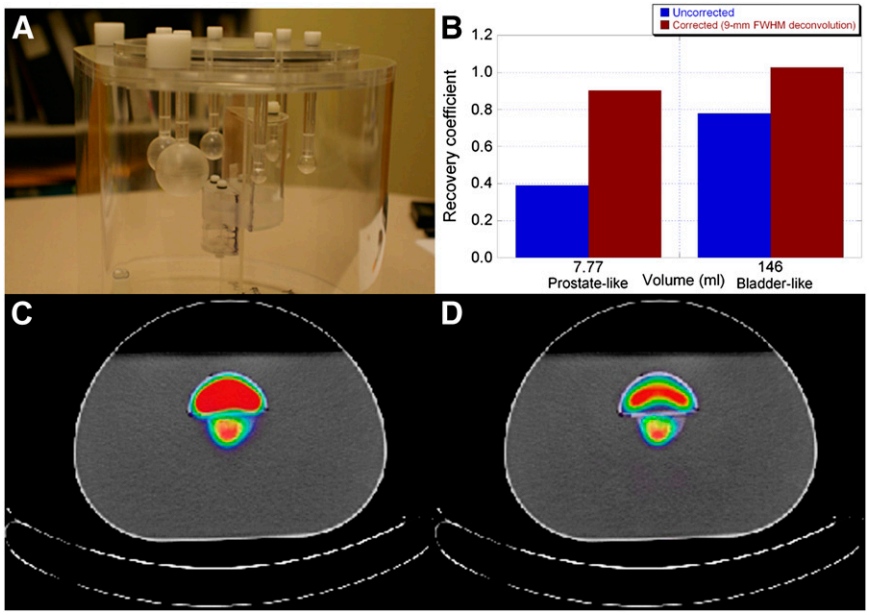

FIGURE 4. Recovery coefficients were measured using modified NEMA/IEC body phantom containing multiple prostate lesions (smallest, 7.77 mL) and bladder lesion (146 mL). (A) Photograph of modified NEMA/IEC body phantom. (B) Chart comparing recovery coefficients in reconstructed images with and without PVE correction. Deconvolution-corrected measurement significantly recovers tracer concentrations, even in small volume (7.77 mL), whereas deconvolution correction effect is less significant in large lesion (146 mL). (C and D) Reconstructed phantom image slices (transaxial view showing 2 filled lesions) uncorrected (C) and corrected (D) by PVE algorithm are also presented.

has not yet been widely adopted in SPECT, primarily because of poor photon statistics and difficulties in applying the necessary physical corrections. We report the validation of a novel approach involving correction factors for 3 major physical perturbations (photon attenuation, scatter, and geometric blurring caused by radionuclide collimators) for SPECT. These physical correction techniques provide a higher target-to-background ratio (*21*). Therefore, even if physical detection efficiency is not improved, an indirect improvement in photon statistics is achieved with the iterative reconstruction algorithm. Dual-modality SPECT/CT technology improves SPECT quantification, particularly with regard to photon attenuation correction.

As we have shown here, tracer quantification that correlates with biologic signatures of tissue, such as PSMA expression for prostate cancer, also requires careful thought on normalization methods to minimize interpatient variability. In the future, we plan to accumulate more patient data and a wider range of Gleason tumor grades, at least to capture some of the grade 5 components. We also plan to explore ways of evaluating the data correlation with other biologic features of prostate cancer, such as spectroscopic biomarkers that can be obtained from MR spectroscopic imaging combined with MRI (*22*).

Tracer quantification in distant metastatic sites is another possibility if we can access these sites for pathologic evaluations. The same analysis we have developed here can be performed to compare in vivo AUV and pathologic tumor status. Eventually, our long-term goal is to develop a validated preoperative imaging-based tumor staging and grading system to alleviate the problems of understaging on prostate biopsy—problems that complicate prostate cancer decision-making, leading to both under- and overtreatment of localized disease. There exists a great need for continuous investigation of novel radiotracers for prostate cancer that specifically target promising biomarkers such as PSMA. Such a radiotracer was reported by Hillier et al. (*23*). We hope our results will thus help invigorate the adoption of quantitative SPECT techniques using these newer tracers.

Gleason score has been considered a predictor of prostate cancer mortality (*24*). However, only recently was it discovered that mortality rates differ among patients with a Gleason score of 7 depending on whether a Gleason pattern of 4 is primary or secondary. For example, Tollefson et al. reported that patients with a primary Gleason grade of 4 (thus, a Gleason score of 4 + 3) have higher rates of biochemical failure, systemic recurrence, and mortality from the disease than those with a primary Gleason grade of 3 (thus, a Gleason score of 3 + 4) (*25*). In our current study, we did not distinguish these 2 different patterns of Gleason score, mainly because of the limited spatial resolution of SPECT even after advanced reconstruction algorithms and PVE correction techniques were used as shown in this article. When we learn of ways to improve the spatial resolution in the future, we will evaluate the different patterns of a Gleason score of 7.

CONCLUSION

We performed phantom and patient studies for quantitative ^{111}In-capromab pendetide SPECT using a commercially available SPECT/CT scanner with an advanced SPECT reconstruction algorithm and PVE correction technique to quantify radiolabeled antibody concentrations in vivo. Our results indicate potential for noninvasive grading of prostate tumors using quantitative ^{111}In-capromab pendetide SPECT/CT. This conclusion will be followed carefully with an expanded patient population including patients with Gleason grades lower than 3 and higher than 4, neither

of which was included in the presented study. In addition, the differences between the primary and secondary Gleason patterns will be evaluated in correlation with the quantitative ^{111}In-capromab pendetide results in future studies.

ACKNOWLEDGMENTS

We thank Marilyn Morrissey and Charisa Thomas at the San Francisco Veterans Affairs Medical Center for technical assistance with the imaging studies. This work was funded in part by National Cancer Institute grant 5 K25 CA114254 and by the University of California Industry–University Cooperative Research Program grant dig 06-10210 with Philips Healthcare.

REFERENCES

1. Jansen FP, Vanderheyden JL. The future of SPECT in a time of PET. *Nucl Med Biol.* 2007;34:733–735.
2. Flux G, Bardies M, Monsieurs M, Savolainen S, Strands SE, Lassmann M. The impact of PET and SPECT on dosimetry for targeted radionuclide therapy. *Z Med Phys.* 2006;16:47–59.
3. Garcia EV. SPECT attenuation correction: an essential tool to realize nuclear cardiology's manifest destiny. *J Nucl Cardiol.* 2007;14:16–24.
4. Manyak MJ. Indium-111 capromab pendetide in the management of recurrent prostate cancer. *Expert Rev Anticancer Ther.* 2008;8:175–181.
5. Nagda SN, Mohideen N, Lo SS, et al. Long-term follow-up of ^{111}In-capromab pendetide (ProstaScint) scan as pretreatment assessment in patients who undergo salvage radiotherapy for rising prostate-specific antigen after radical prostatectomy for prostate cancer. *Int J Radiat Oncol Biol Phys.* 2007;67:834–840.
6. Fair WR, Israeli RS, Heston WD. Prostate-specific membrane antigen. *Prostate.* 1997;32:140–148.
7. Sweat SD, Pacelli A, Murphy GP, Bostwick DG. Prostate-specific membrane antigen expression is greatest in prostate adenocarcinoma and lymph node metastases. *Urology.* 1998;52:637–640.
8. Seo Y, Mari C, Hasegawa BH. Technological development and advances in single-photon emission computed tomography/computed tomography. *Semin Nucl Med.* 2008;38:177–198.
9. Seo Y, Wong KH, Hasegawa BH. Calculation and validation of the use of effective attenuation correction for attenuation correction in In-111 SPECT. *Med Phys.* 2005;32:3628–3635.
10. Seo Y, Wong KH, Sun M, Franc BL, Hawkins RA, Hasegawa BH. Correction of photon attenuation and collimator response for a body-contouring SPECT/CT imaging system. *J Nucl Med.* 2005;46:868–877.
11. Song X, Segars WP, Du Y, Tsui BM, Frey EC. Fast modelling of the collimator-detector response in Monte Carlo simulation of SPECT imaging using the angular response function. *Phys Med Biol.* 2005;50:1791–1804.
12. Vandervoort E, Celler A, Harrop R. Implementation of an iterative scatter correction, the influence of attenuation map quality and their effect on absolute quantitation in SPECT. *Phys Med Biol.* 2007;52:1527–1545.
13. Celler A, Dixon KL, Chang Z, Blinder S, Powe J, Harrop R. Problems created in attenuation-corrected SPECT images by artifacts in attenuation maps: a simulation study. *J Nucl Med.* 2005;46:335–343.
14. Tsui BM, Gullberg GT, Edgerton ER, et al. Correction of nonuniform attenuation in cardiac SPECT imaging. *J Nucl Med.* 1989;30:497–507.
15. Teo BK, Seo Y, Bacharach SL, et al. Partial-volume correction in PET: validation of an iterative postreconstruction method with phantom and patient data. *J Nucl Med.* 2007;48:802–810.
16. Soret M, Bacharach SL, Buvat I. Partial-volume effect in PET tumor imaging. *J Nucl Med.* 2007;48:932–945.
17. Seo Y. Prostate-bladder phantom for radionuclide imaging research. In: *Nuclear Science Symposium Conference Record.* Piscataway, NJ: IEEE; 2008:4820–4822.
18. Huang SC. Anatomy of SUV: standardized uptake value. *Nucl Med Biol.* 2000;27:643–646.
19. Zakian KL, Sircar K, Hricak H, et al. Correlation of proton MR spectroscopic imaging with Gleason score based on step-section pathologic analysis after radical prostatectomy. *Radiology.* 2005;234:804–814.
20. Gleason DF. Histologic grading of prostate cancer: a perspective. *Hum Pathol.* 1992;23:273–279.
21. Seo Y, Franc BL, Hawkins RA, Wong KH, Hasegawa BH. Progress in SPECT/CT imaging of prostate cancer. *Technol Cancer Res Treat.* 2006;5:329–336.
22. Swanson MG, Vigneron DB, Tran TK, Kurhanewicz J. Magnetic resonance imaging and spectroscopic imaging of prostate cancer. *Cancer Invest.* 2001;19:510–523.
23. Hillier SM, Maresca KP, Femia FJ, et al. Preclinical evaluation of novel glutamate-urea-lysine analogues that target prostate-specific membrane antigen as molecular imaging pharmaceuticals for prostate cancer. *Cancer Res.* 2009;69:6932–6940.
24. Andren O, Fall K, Franzen L, Andersson SO, Johansson JE, Rubin MA. How well does the Gleason score predict prostate cancer death? A 20-year followup of a population based cohort in Sweden. *J Urol.* 2006;175:1337–1340.
25. Tollefson MK, Leibovich BC, Slezak JM, Zincke H, Blute ML. Long-term prognostic significance of primary Gleason pattern in patients with Gleason score 7 prostate cancer: impact on prostate cancer specific survival. *J Urol.* 2006;175:547–551.

The Journal of NUCLEAR MEDICINE

In Vivo Tumor Grading of Prostate Cancer Using Quantitative ^{111}In-Capromab Pendetide SPECT/CT

Youngho Seo, Carina Mari Aparici, Matthew R. Cooperberg, Badrinath R. Konety and Randall A. Hawkins

J Nucl Med. 2010;51:31-36.
Published online: December 15, 2009.
Doi: 10.2967/jnumed.109.067108

The Journal of Nuclear Medicine is published monthly.
SNMMI | Society of Nuclear Medicine and Molecular Imaging
1850 Samuel Morse Drive, Reston, VA 20190.
(Print ISSN: 0161-5505, Online ISSN: 2159-662X)

SNMMI SOCIETY OF NUCLEAR MEDICINE AND MOLECULAR IMAGING